Steel and Composite Structures, *Vol. 23, No. 1 (2017) 107-114*
DOI: https://doi.org/10.12989/scs.2017.23.1.107

Design of stepwise foam claddings subjected to air-blast based on Voronoi model

Minzu Liang [a], Fangyun Lu [b], Guodong Zhang [c] and Xiangyu Li [*]

College of Science, National University of Defense Technology, 410073 Changsha, P.R. China

(Received September 12, 2016, Revised November 29, 2016, Accepted December 14, 2016)

Abstract. Design of stepwise foam claddings subjected to air-blast is performed based on random Voronoialgorithm. FE models are constructed using the random Voronoialgorithm, and numerical analysis is carried out to simulate deformation mode and energy absorption of the cladding by the ABAQUS/Explicit software. The FE model is validated by test result, and good agreement is achieved. The deformation patterns are presented to give an insight into the influences of distribution on deformation mechanisms. The energy absorbed by the stepwise foam cladding is examined, and the parameter effects, including layer number, gradient, and blast loading, are discussed. Results indicate that the energy absorption capacity increases with the number of layer, gradient degree, and blast pressure increasing.

Keywords: Voronoi; air-blast; foam; cladding

1. Introduction

Foams are a new class of ultra-light multi-functional materials with the ability to undergo large deformation at a nearly constant plateau stress, and thus can absorb a large amount of kinetic energy before collapsing to a more stable configuration (Gibson and Ashby 1997, Xue and Hutchinson 2006, Li *et al*. 2015a, Chuda-Kowalska and Garstecki 2016, Yurddaskal and Baba 2016). Foams have been attached as sacrificial layers to protect structures, machines and infrastructure against dynamic events. The cladding is supposed to be damaged during impact or blast loading, thereby mitigating the amount of damage for main structures (protected objects) (Gama *et al*. 2001, Mines 2004). Their properties assist in dispersing energy and impulse transmitted into the structure, and thus protects objects located behind them (Xie *et al*. 2014).

Blast responses of foam cladding were well studied, providing useful guide for design of protective structures against blast loading (Main and Gazonas 2008, Shen *et al*. 2013). Guruprasad and Mukherjee (2000a, b) investigated performance of sacrificial layer under blast loading by experimental and analytical methods. Results showed that layered sacrificial claddings were very effective in energy absorption and they had a predictable behavior under blast loading. Hanssen *et al*. (2002) proposed an analytical solution based on shock-wave theory to explain the phenomenon that energy and impulse transfer to pendulum increased by adding a foam panel in the experiments. An analytical Load-Cladding-Structure (LCS) model was proposed to investigate deformation of foam subjected to blast loading by Ma and Ye (Ma and Ye 2007, Ye and Ma 2007). Karagiozova *et al*. (2010) developed an analytical model to reveal the characteristic features of a foam compaction under blast loading. Merrett *et al*. (2013) reported results from impact and blast loading experiments on aluminum foams. They found the blast tests resulted in uniaxial ductile crushing of the foam but indicated no evidence of shock at low blast loading. Aleyaasin *et al*. (2015) derived a new method of accounting for fluid-structure interaction (FSI) in the foam cladding.

Most available mechanical models are usually based on idealized unit cell structures, and are not able to account for the natural variations in microstructure that are typical for most foam structures. The random Voronoi technique is a smart tool to simulate the deformation process and dynamic response of foam material and structure. Zhu *et al*. (2001, 2006) constructed random Voronoi structures to determine the effect of cell irregularity on foam materials. Zheng *et al*. (2014) simulated the dynamic crushing process of foams using 2D and 3DVoronoi structures. Ajdari *et al*. (2011) introduced the Voronoi technique to investigate the energy absorption of honeycombs with constant and functionally graded density. Liao *et al*. (2013) proposed a method to obtain the local strain field of foam materials using the Voronoi technique. Zhang *et al*. (2016) simulated and analyzed dynamic response of cellular materials with density gradient based on the Voronoi model.

In order to achieve a better blast response, stepwise foam claddings have been recently receiving an increasing attention (Wang *et al*. 2013, Zheng *et al*. 2013, 2016, Karagiozova and Alves 2014, Shen *et al*. 2014, Darvizeh and Davey 2015, Wang *et al*. 2015, Zhang *et al*. 2016). Since the properties of stepwise foam claddings can be

*Corresponding author, Professor,
E-mail: xiangyulee@nudt.edu.cn
[a] Ph.D. Student, E-mail: mzliang@nudt.edu.cn
[b] Professor, E-mail: fylu@nudt.edu.cn
[c] Ph.D. Student, E-mail: krippin@163.com

ISSN: 1229-9367 (Print), 1598-6233 (Online)

designed and controlled, they show great potential to absorb more energy and improving the overall blast resistance of protective structures (Li *et al*. 2015).

In this paper, random Voronoi model is used to investigate optimization design of stepwise foam claddings subjected to air-blast. Deformation process of the foam cladding is investigated in details using the Voronoi model. Meanwhile, deformation mechanisms of the cladding with different distributions are proposed. In addition, the energy absorbed by the stepwise foam cladding is examined, and the parameter effects, including layer number, gradient, and blast loading, are investigated. The results will help to understand the performance and the mechanisms of stepwise foam claddings under blast loading and provide a guideline for a better structure design. Firstly, random Voronoi algorithm is employed to create stepwise foam cladding. The finite element (FE) model is validated by the experimental result. Then, the deformation mode and energy absorption of the stepwise foam cladding under air-blast are studied using ABAQUS/Explicit software. Finally, deformation and energy absorption of the cladding with various distributions are discussed.

2. Random Voronoi algorithm

The random Voronoi algorithm was applied to generate closed-cell foams with a uniform cell-wall thickness. Firstly, N nuclei are randomly generated in a given area A based on the principle that the minimum distance between any two nuclei is constrained to be larger than a given distance $\delta_{\min}$

$$\delta_{\min} = (1-k)\delta_0 \tag{1}$$

where k is the degree of cell irregularity, and $k = 0.2$ is used in this study. δ_0 is the distance between any two adjacent nuclei which is given by

$$\delta_0 = \sqrt{2A/\sqrt{3}N} \tag{2}$$

Secondly, these generated nuclei are copied to the surrounding neighboring regions by translation. Thirdly, the Delaunay triangulation and the Voronoi diagram are constructed. As shown in Fig. 1, a Voronoi cell contains all points that are closer to its data point than any other data points in the set. Finally, the periodic Voronoi structure is constructed after out of the given area A is deleted. The relative density of the foam is defined as

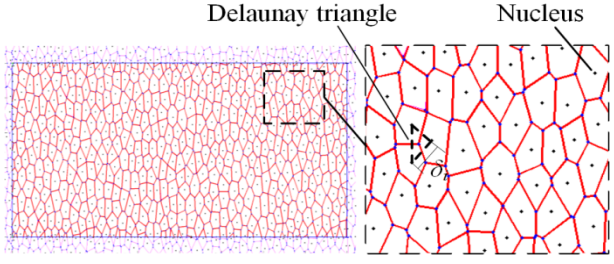

Fig. 1 Random Voronoi model

$$\rho = \rho_f / \rho_s = \sum h_j l_j / A, \tag{3}$$

where ρ_f is the density of the foam, ρ_s the density of the based material. l_j is the cell wall length and h_j the corresponding wall thickness.

3. FE model

Numerical simulations are performed by ABAQUS/Explicit software. As shown in Fig. 2, the foam cladding is sandwiched between two rigid plates. The rigid plate at distal end is fixed. The TNT charge to be detonated is held in place at a horizontal standoff distance relative to the front of the rigid plate at the proximal end. The FE model of the cladding is constructed in an area of 100×400 mm^2. The structure block is divided into two cladding. The density gradient, g, was defined as

$$g = \rho_1 / \rho_2, \tag{4}$$

where the ρ_1 and ρ_2 are the relative density of layers. The gradient is positive if the soft layer locates near the blast end. To study the effect of the gradient on dynamic response of foam claddings, various gradients, namely, -0.5, -0.3, 0 (uniform foam), 0.3, 0.5, were considered. The thickness of foam cells is uniform. The difference between two layers is the size distribution of cells. The relative density of the layer is high when the cell size is small.

The aluminum cell wall is assumed to be elastic-perfectly plastic model with density $\rho_s = 2700$ kg/m^3, Young modulus $E_s = 69$ GPa, Poisson ratio $\gamma_s = 0.3$ and yield stress $\sigma_{ys} = 170$ MPa. The foam cladding is meshed using Lagrange elements. The FE model consists of 56612 elements. The average mesh size is 0.6 mm for the foam cladding and 0.8 mm for the explosive charge. The effect of mesh size on the crushing wave motion is shown in Fig. 3. The wave motion is slightly influenced by the mesh size when the size is smaller than 0.8 mm. Mesh size sensitivity investigation reveals that further refinements do not improve the accuracy of the calculation appreciably. The cell wall is meshed by using a type of ABAQUS shell element S4R.Self-contact is applied to all the cell surfaces; meanwhile, general contact is considered between the Voronoi structure and the front-plates with a friction coefficient of 0.02 (Zheng *et al*. 2005, 2014). The Jones-Wilkins-Lee (JWL) equation is used to describe the detonation products of TNT explosives. This equation defines the pressure field as a function of relative volume and internal energy per initial volume as

$$\begin{aligned} p = {} & A\left(1-\frac{\omega\rho_e}{R_1\rho_{e0}}\right)e^{-R_1\frac{\rho_e}{\rho_{e0}}} \\ & + B\left(1-\frac{\omega\rho_e}{R_2\rho_{e0}}\right)e^{-R_2\frac{\rho_e}{\rho_{e0}}} + \frac{\omega\rho_e}{\rho_{e0}}E_{m0}, \end{aligned} \tag{5}$$

where p is the detonation pressure, ρ_e is the explosive density, ρ_{e0} is the initial explosive density, and A, B, R_1, R_2 and ω are material constants. The parameters of the explosive are listed in Table 1 (Dobratz 1981).

Table 1 JWL model parameters of the TNT explosive

Explosive	Detonation wave speed, D (m/s)	A	B	ω	R_1	R_2	Detonation energy density, E_{m0} (J/m^3)	Pre-detonation bulk modulus
TNT	6930	3.74	0.032	0.3	4.15	0.95	70	1.0

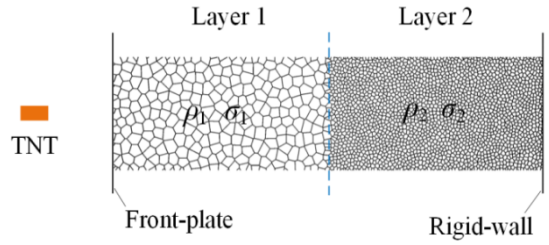

Fig. 2 FE model based on the random Voronoi model

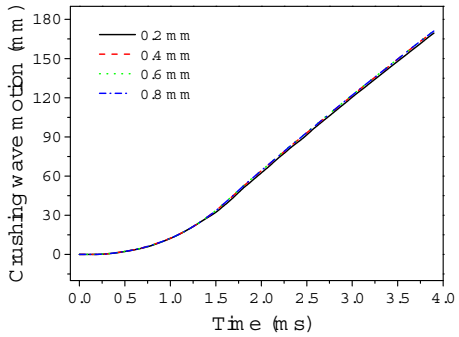

Fig. 3The effect of mesh size on the crushing wave motion

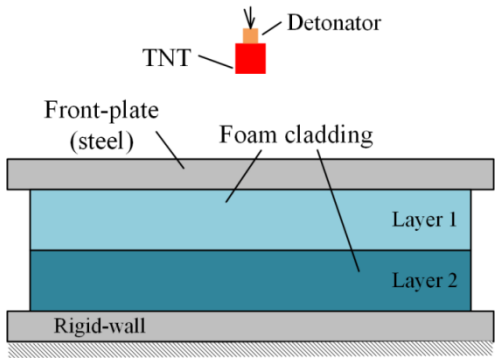

Fig. 4 A sketch of the testing setup

4. Validation of FE model

To verify the material properties, boundary and contact conditions in the FE model, the result was compared to the blast result. The test procedure is shown in Fig. 4. The stepwise foam cladding was sandwiched between two steel plates. The TNT explosive with cubic shape was held centrally on the top face of front-plate place at a vertical standoff distance of 200 mm, and was detonated at its apex with a detonator. The steel-plates have a square of 160 mm with a 10 mm thickness. The front-plate was placed on the foam claddings in order to transmit detonation pressure for the explosive. The claddings have a square of 120 mm and a thickness of 20 mm, which was cut to shape by electro-discharge machine to minimize damage to the cell edges. Then the claddings were annealed at 393 K for 1 hour to relieve residual stresses in the foams during the manufacturing of the base material and the machining process.

Table 2 Comparisons of cross-section thicknesses of deformed specimens

	Positive foam /(mm)		Negative foam /(mm)	
	Layer 1	Layer 2	Layer 1	Layer 2
Experimental results	9	20	17	10
Simulation predictions	9.2	20	17.1	9.9

When the foam cladding is positive gradient, the soft layer was placed on the hard layer next to blast end in the test. Fig. 5 compares the cross-section of deformed claddings from the simulation and the test. The layer 1 has collapsed more than a half, whereas the layer 2 has not deformed. It is indicated that the compaction initiates from the blast end and then propagates to the fixed end when the gradient is positive. This result agrees well with the numerical predictions. The test validates the FE model is reasonable. Table 2 compares the cross-section thicknesses of deformed specimens. A good agreement is achieved between the experimental results and simulation predictions.

5. Results and discussion

5.1 Deformation mode

The compression processes of the cladding under quasi-static and dynamic loading are different in the result of the different deformation modes (Liu *et al*. 2009, Karagiozova and Alves 2015). The deformation modes of foam cladding

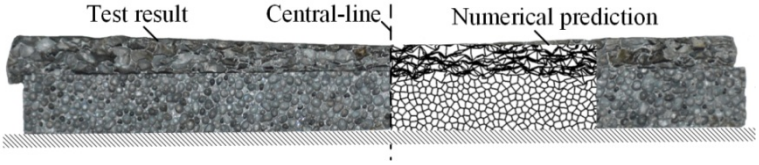

Fig. 5 Comparisons of the cross-sections of deformed claddings between the test result and simulation prediction

are complicated under blast loading, and related studies are limited (Karagiozova *et al*. 2010, Aleyaasin *et al*. 2015). The macroscopic deformation of foam is always classified into three modes. Zheng *et al*. (2005) called these three modes the quasi-static mode, transitional mode, and dynamic mode, respectively; and Ma *et al*. (2009) called the three modes random mode, transitional mode, and progressive mode, respectively. These modes are dependent on the impact velocity of the front-plate. Mode I appears at a low impact velocity. The deformation is localized in crushing bands of collapsing cells, which are randomly distributed. Mode II appears at a moderate impact velocity. The crushing bands concentrate near the impact end because of inertia effect. Mode III appears at a high impact velocity. The deformation is highly localized at the impact end and progressive cell crushing is observed to propagate like a shock wave. Hönig and Stronge (2002) formulated a critical impact velocity for the development of a steady mode III based on wave-trapping theory

$$v_{cr} = \int_0^{\varepsilon_{cr}} c(\varepsilon) d\varepsilon, \tag{6}$$

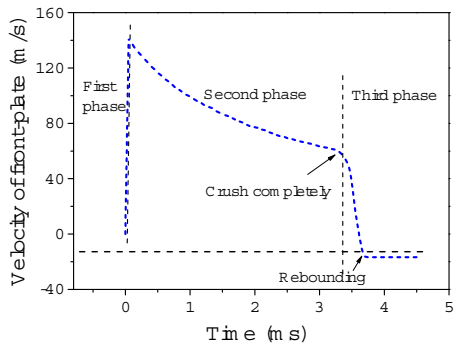

Fig. 6 The velocity history of the front-plate

where $c(\varepsilon) = [(d\sigma/d\varepsilon)/\rho_0]^{1/2}$ is the velocity of stress wave in the materials, ε_{cr} is the strain where $d\sigma/d\varepsilon = 0$.

As blast loading is short and monotonically decreasing, there exists a maximum velocity for the front-plate and compaction part. As shown in Fig. 6, the motion of the front-plate can generally be described in three main phases. The velocity of the front-plate increases rapidly in a very short period, and reaches a maximum velocity in the first phase. Based on the momentum conservation, the maximum velocity can be obtained by

$$v_{\max} = \frac{\int p(t)dt}{m_f}, \tag{7}$$

where $p(t)$ is the blast pressure, m_f is the mass of the front-plate. In the second phase, the front-plate compresses the foam and the velocity decreases gradually. The mode III occurs when the impact velocity exceeds a critical value. Therefore, the foam always appears mode III at the early stage of the second phase. In the last phase, the front-plate rebounds back. As shown in Fig. 7(a), the mode maintains mode III in the deformation process if the blast pressure is high. If the blast pressure is low, the mode changes from mode III to mode II in the second phase (Fig. 7(b)). This is because the velocity is lower than the critical velocity. The mode will change to mode I if the velocity decreases continually.

5.2 Distribution design

The deformation patterns are presented here to give an insight into the effects of distribution on deformation mechanisms of the foam cladding. The foam claddings with positive and negative gradients are shown in Fig. 8. The crushing stress on the shock wave front is sensitive to the blast pressure. The crushing stress is up to 3.2 MPa when the blast pressure is 20.13 MPa. The initial velocity of the

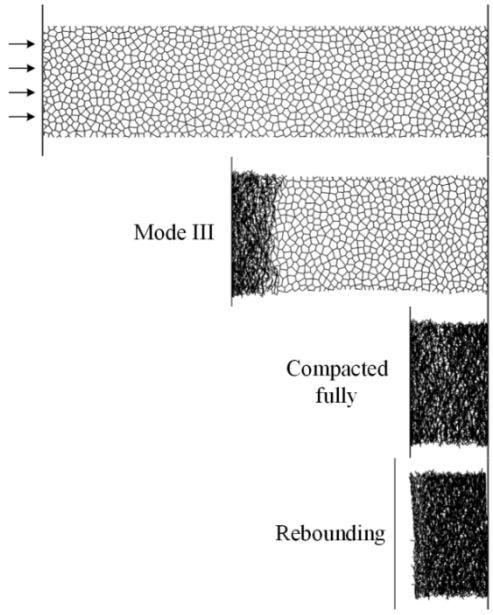

(a) Peak pressure of air-blast: 20.13 MPa

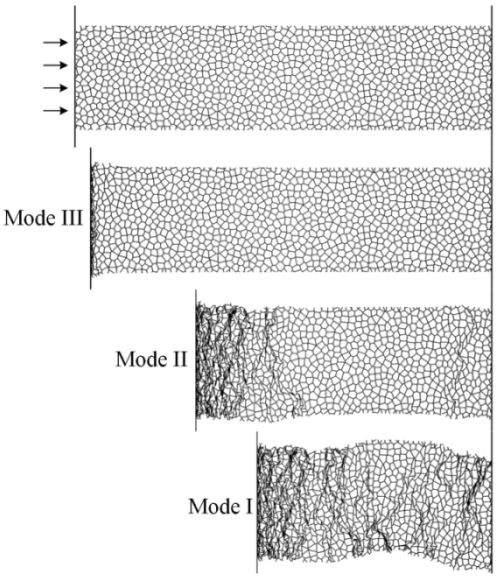

(b) Peak pressure of air-blast: 9.43 MPa

Fig. 7 Deformation of foam cladding subjected to blast loading

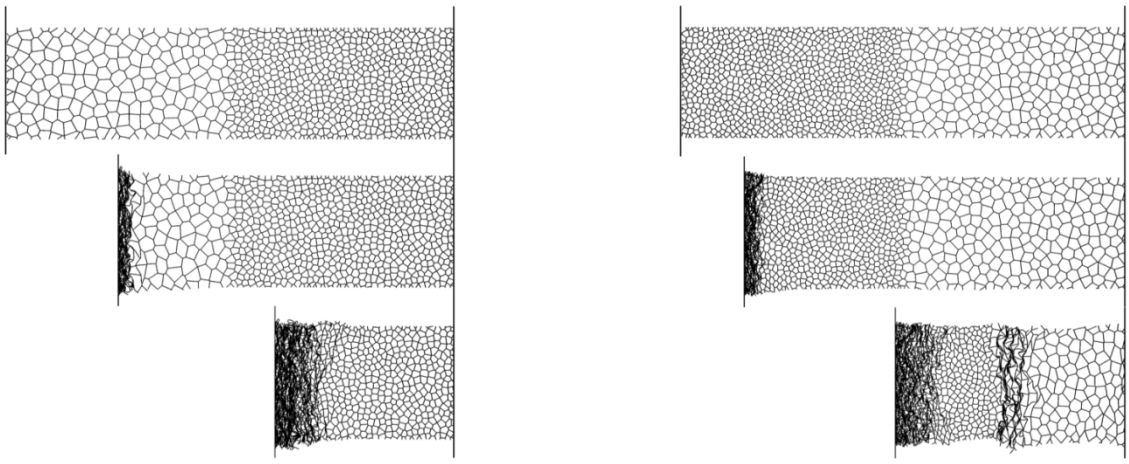

(a) Positive gradient (b) Negative gradient

Fig. 8 Deformation of the positive and negative gradient cladding

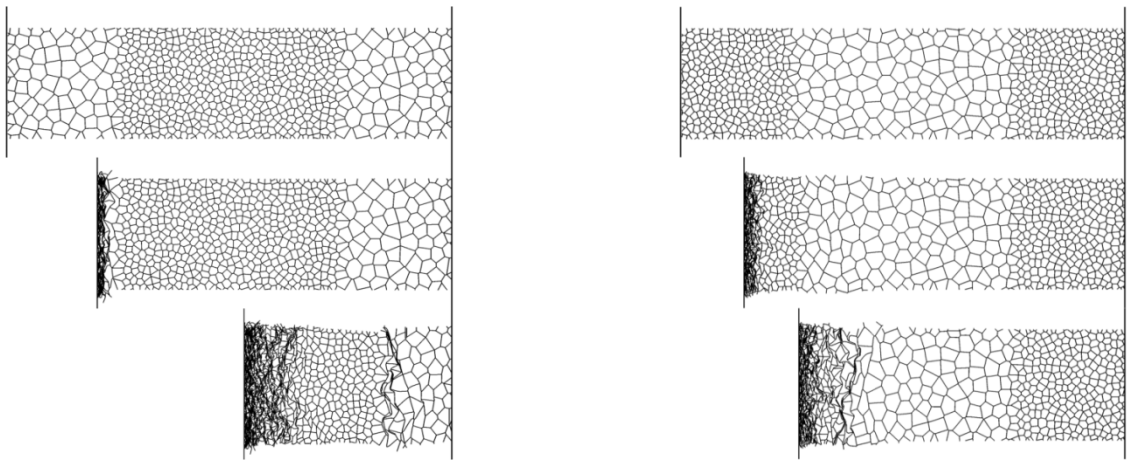

(a) Middle-high (b) Middle-low

Fig. 9 Deformation of cladding with middle-high and middle-low distributions

front-plate subjected to blast loading is about 140 m/s. The densification strain of the foam is approximately 0.75. The density of the compacted part is 0.86 g/cm^3.

The compaction wave initiates at the blast end and then propagates to the fixed end when the gradient is positive. As it can be seen from Fig. 8(b) for the deformation process of the cladding with negative gradient, the blast end crushes firstly, and then compaction wave starts at the proximal end of the second layer when stress wave reaches the interface between these two layers. The double shock fronts propagate to the fixed end in the same direction. As shown in Fig. 9, the deformation patterns of middle-high and middle-low distributions are compared. For the middle-high distribution, the compaction wave commences at the low-density layer next to the blast end firstly. When compaction wave reaches the high-density layer, an obvious compaction begins at the proximal end of the low-density layer next to the fixed end. For the middle-low distribution, the situation is similar to the cladding with the negative cladding before the crushing of the last layer next to the fixed end. Fig. 10 depicts the deformation process of the claddings with interval distributions. For the cladding with low-high interval distribution, the blast end crushes firstly, then, the proximal end of the third layer (low-density layer) begins to crush after the crushing arrives the second part (high-density layer). The process of the cladding with high-low interval distribution can be considered as double processes of the negative cladding.

When the foam is uniform, the material at the blast end is fully compacted while the rest part remains undeformed. The crushed and undeformed parts are separated by a fast propagating thin layer, termed as shock front. There is only one shock wave propagating from the blast end to fixed end during the completely crushing process. When the gradient is positive, the phenomenon is coincided with uniform foam. When the gradient is negative, the hard layer is placed at the blast end. The densification appears in layer 1 at blast end firstly. Subsequently compaction starts in layer 2 at the end near to layer 1.

The deformation modes for crushing of double-layer foams are discussed. Assuming that densities of layer 1 and layer 2 are ρ_1 and ρ_2, respectively, and corresponding plateau stresses areσ_1 and σ_2.The layer 1 is near to blast end, and the layer 2 is at the distal end.

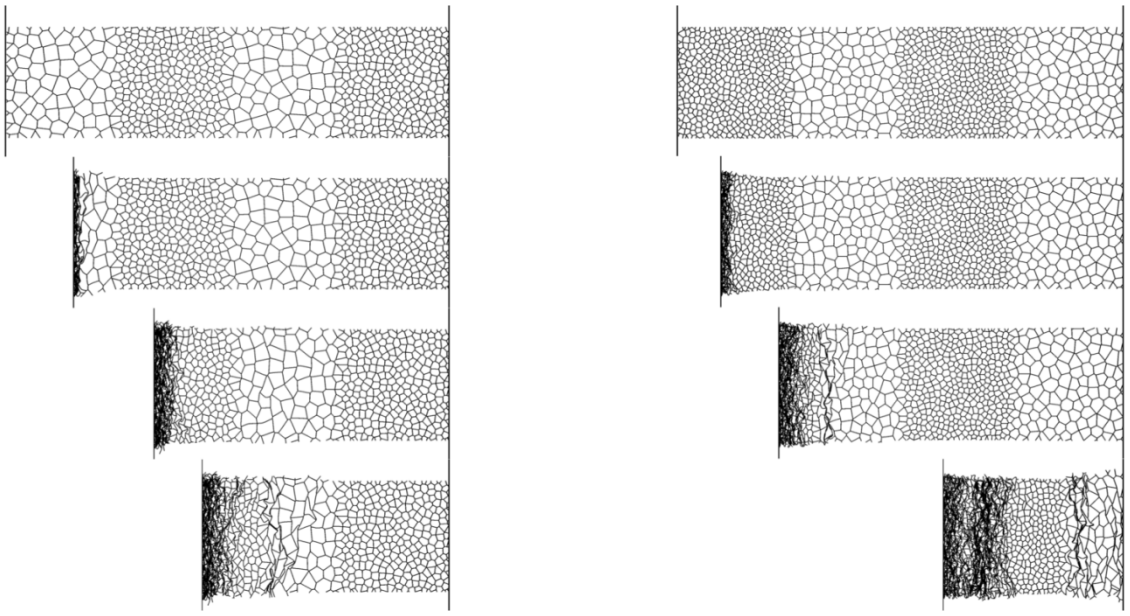

(a) Low-high interval (b) High-low interval

Fig. 10 Deformation of cladding with interval distributions

When the gradient is positive, the soft layer is placed at the proximal end, $\sigma_1 < \sigma_2$. The proximal end deforms immediately after blast wave reaches. However, according to uniform foam analysis above, the reaction stress at interface between the foam layers is quasi-static plateau stress of soft layer σ_1. Therefore, the reaction stress at the interface is still below its quasi-static plateau stress so that hard layer remains undeformed during the entire crushing process of the soft layer. Therefore, densification occurs from the proximal end and then gradually propagates to the distal end.

When the gradient is negative, the hard layer is placed at the proximal end, $\sigma_1 > \sigma_2$. The reaction stress at interface between two layers is equal to the quasi-static plateau stress of hard layer, σ_1, which exceeds quasi-static plateau stress of soft layer. The Young's modulus of the R-PP-L model material approaches infinite; therefore, the critical velocity is approximate to zero. Hence, the blast end crushes firstly, and then compaction wave starts at the proximal end of layer 2 when stress wave reaches the interface between two layers.

6. Energy absorption

It is of practical interest to determine the energy absorption of stepwise foam cladding subjected to blast load. Assuming the elastic deformation energy of the aluminium foam is negligible, the quasi-static energy absorption can be obtained by

$$E_0 = \sum \sigma_i \varepsilon_{id} \xi_i, \tag{8}$$

where i is the layer no., ξ_i is the Lagrangian coordinate of compaction wave front, σ_i, and ε_{id} are quasi-static plateau stress, and densification strain of the layer i, respectively. The energy absorption of the cladding under blast loading can be calculated by

$$E_0 = \sum (\sigma_i + \sigma_{id}) \varepsilon_{id} \xi_i / 2. \tag{9}$$

Conservations of mass and momentum at the compaction wave front and idealizing the cladding as the R-PP-L model, the crushing stress σ_{id} as a function of velocity of shock front v is given as (Reid and Peng 1997, Tan *et al*. 2005)

$$\sigma_{id} = \sigma_i + \frac{\rho_i v^2}{\varepsilon_{id}}, \tag{10}$$

where ρ_i is the density of the layer i. Substituting Eqs. (8) and (10) into Eq. (9) gives

$$E = E_0 + \sum \xi_i \rho_i v(\xi)^2 / 2. \tag{11}$$

Fig. 11 depicts layer number effects on energy absorption of foam cladding. With the number of layer increasing, the energy absorption capacity increases. However, the increment decreases when the cladding is greater than three layers. It implied that the continuously graded foam is approximately substituted with the stepwise foam cladding in energy absorption (Zhou *et al*. 2016). As the stepwise foam claddings can be designed and controlled easily, they show great potential to be used in protective structures. As shown in Fig. 12, the influence of the gradient on energy absorption is investigated. It is shown that the greater the cladding gradient, the higher the energy absorption. The energy absorption of the positive gradient is obviously larger than that of the other gradient distributions; and the energy of the negative one has the smallest value. Fig. 13 demonstrates the relationship between displacement

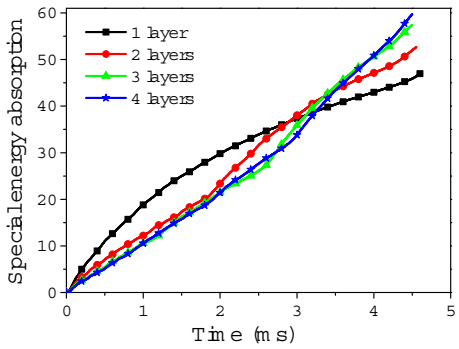

Fig. 11 Influence of the layer numbers on energy absorption under peak pressure of 20.13 MPa

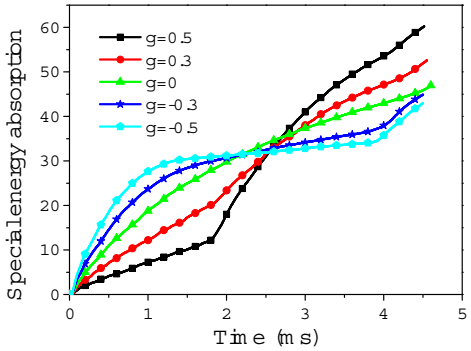

Fig. 12 Influence of the gradient on energy absorption of the cladding with two layers

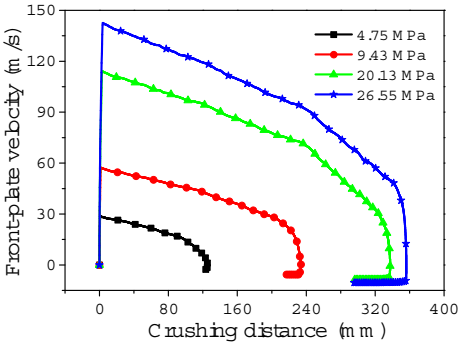

Fig. 13 Crushed distance and velocity of the front-plate

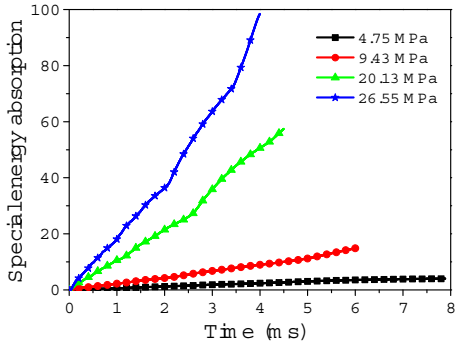

Fig. 14 Influence of the blast pressure on energy absorption foam cladding with three layers

and velocity of front-plate under different blast loading. It can be observed that the crushed distance increases with increasing of blast loading. When the initial peak pressure are 20.13 MPa and 26.55 MPa, the velocity of front-plate decreases fast at the end of crushing. Because its kinetic energy exceeds energy absorption capacity of the cladding, the front-plate and compaction part impact the fixed end directly at last. As shown in Fig. 14, energy absorption capacity increases with blast pressure. The relationship between the energy absorption trend and blast pressure can be explained as follows. According to Eq. (7), higher-pressure leads to higher-maximum velocity, which leads to higher-crushing stress based on Eq. (10). Considering Eq. (11), the crushing resistance is related to velocity-dependent dynamic enhancement and crushed displacement. Hence, energy absorption capacity increases with blast pressure due to higher dynamic plateau stress and crushed displacement under higher blast pressure.

7. Conclusions

FE models are constructed by the random Voronoi algorithm, and numerical simulations are carried out to investigate deformation mode and energy absorption of the foam cladding by the ABAQUS/Explicit software.

- The deformation process of the cladding simultaneously includes three modes, which are dependent on the impact velocity of the front-plate.
- The deformation patterns are presented to study the effects of distributions on deformation mechanisms. The layer at blast end begins to compact firstly. If a soft layer is placed ahead, the subsequent layer will not deform until the compaction wave reaches. If a hard layer is placed ahead, the subsequent layer crushes with the former layer simultaneously.
- The energy absorption capacity increases with the number of layer, gradient degree, and blast pressure increasing.

Acknowledgments

The authors would like to acknowledge financial supported by the China National Natural Science Funding (No. 11132012).

References

Ajdari, A., Nayeb-Hashemi, H. and Vaziri, A. (2011), "Dynamic crushing and energy absorption of regular, irregular and functionally graded cellular structures", *Int. J. Solids Struct.*, **48**(3-4), 506-516.

Aleyaasin, M., Harrigan, J.J. and Reid, S.R. (2015), "Air-blast response of cellular material with a face plate: An analytical–numerical approach", *Int. J. Mech. Sci.*, **91**, 64-70.

Chuda-Kowalska, M. and Garstecki, A. (2016), "Experimental study of anisotropic behavior of PU foam used in sandwich panels", *Steel Compos. Struct., Int. J.*, **20**(1), 43-56.

Darvizeh, R. and Davey, K. (2015), "A transport approach for analysis of shock waves in cellular materials", *Int. J. Impact Eng.*, **82**, 59-73.

Dobratz, B.M. (1981), "Properties of chemical explosives and explosive simulants", *International Journal of Neuroscience*, **51**(3-4), 339-340.

Gama, B.A., Bogetti, T.A., Fink, B.K., Yu, C.-J., Dennis Claar, T., Eifert, H.H. and Gillespie, Jr. J.W. (2001), "Aluminum foam integral armor: a new dimension in armor design", *Compos. Struct.*, **52**(3-4), 381-395.

Gibson, L.J. and Ashby, M.F. (1997), *Cellular Solids: Structure and Properties*, Cambridge University Press, Cambridge, UK.

Guruprasad, S. and Mukherjee, A. (2000a), "Layered sacrificial claddings under blast loading Part I — Analytical studies", *Int. J. Impact Eng.*, **24**(9), 957-973.

Guruprasad, S. and Mukherjee, A. (2000b), "Layered sacrificial claddings under blast loading Part II — Experimental studies", *Int. J. Impact Eng.*, **24**(9), 975-984.

Hanssen, A.G., Enstock, L. and Langseth, M. (2002), "Close-range blast loading of aluminium foam panels", *Int. J. Impact Eng.*, **27**(6), 593-618.

Hönig, A. and Stronge, W.J. (2002), "In-plane dynamic crushing of honeycomb. Part II: Application to impact", *Int. J. Mech. Sci.*, **44**(8), 1697-1714.

Karagiozova, D. and Alves, M. (2014), "Compaction of a double-layered metal foam block impacting a rigid wall", *Int. J. Solids Struct.*, **51**(13), 2424-2438.

Karagiozova, D. and Alves, M. (2015), "Propagation of compaction waves in cellular materials with continuously varying density", *Int. J. Solids Struct.*, **71**, 323-337.

Karagiozova, D., Langdon, G.S. and Nurick, G.N. (2010), "Blast attenuation in Cymat foam core sacrificial claddings", *Int. J. Mech. Sci.*, **52**(5), 758-776.

Li, S., Lu, G., Wang, Z., Zhao, L. and Wu, G. (2015a), "Finite element simulation of metallic cylindrical sandwich shells with graded aluminum tubular cores subjected to internal blast loading", *Int. J. Mech. Sci.*, **96-97**, 1-12.

Li, F., Sun, G., Huang, X., Rong, J. and Li, Q. (2015b), "Multiobjective robust optimization for crashworthiness design of foam filled thin-walled structures with random and interval uncertainties", *Eng. Struct.*, **88**, 111-124.

Liao, S., Zheng, Z. and Yu, J. (2013), "Dynamic crushing of 2D cellular structures: Local strain field and shock wave velocity", *Int. J. Impact Eng.*, **57**, 7-16.

Liu, Y.D., Yu, J.L., Zheng, Z.J. and Li, J.R. (2009), "A numerical study on the rate sensitivity of cellular metals", *Int. J. Solids Struct.*, **46**(22-23), 3988-3998.

Ma, G.W. and Ye, Z.Q. (2007), "Analysis of foam claddings for blast alleviation", *Int. J. Impact Eng.*, **34**(1), 60-70.

Ma, G.W., Ye, Z.Q. and Shao, Z.S. (2009), "Modeling loading rate effect on crushing stress of metallic cellular materials", *Int. J. Impact Eng.*, **36**(6), 775-782.

Main, J.A. and Gazonas, G.A. (2008), "Uniaxial crushing of sandwich plates under air blast: Influence of mass distribution", *Int. J. Solids Struct.*, **45**(7-8), 2297-2321.

Merrett, R.P., Langdon, G.S. and Theobald, M.D. (2013), "The blast and impact loading of aluminium foam", *Mater. Des.*, **44**, 311-319.

Mines, R.A.W. (2004), "A one-dimensional stress wave analysis of a lightweight composite armour", *Compos. Struct.*, **64**(1), 55-62.

Reid, S.R. and Peng, C. (1997), "Dynamic uniaxial crushing of wood", *Int. J. Impact Eng.*, **19**(5-6), 531-570.

Shen, C.J., Lu, G. and Yu, T.X. (2014), "Investigation into the behavior of a graded cellular rod under impact", *Int. J. Impact Eng.*, **74**, 92-106.

Shen, J., Lu, G., Zhao, L. and Zhang, Q. (2013), "Short sandwich tubes subjected to internal explosive loading", *Eng. Struct.*, **55**, 56-65.

Tan, P.J., Reid, S.R., Harrigan, J.J., Zou, Z. and Li, S. (2005), "Dynamic compressive strength properties of aluminium foams. Part II—'shock' theory and comparison with experimental data and numerical models", *J. Mech. Phys. Solids*, **53**(10), 2206-2230.

Wang, X., Zheng, Z. and Yu, J. (2013), "Crashworthiness design of density-graded cellular metals", *Theor. Appl. Mech. Lett.*, **3**(3), 031001-031001-031005.

Wang, P., Xu, S., Li, Z., Yang, J., Zhang, C., Zheng, H. and Hu, S. (2015), "Experimental investigation on the strain-rate effect and inertia effect of closed-cell aluminum foam subjected to dynamic loading", *Mater. Sci. Eng., A*, **620**, 253-261.

Xie, Z., Yan, Q. and Li, X. (2014), "Investigation on low velocity impact on a foam core composite sandwich panel", *Steel Compos. Struct., Int. J.*, **17**(2), 159-172.

Xue, Z. and Hutchinson, J.W. (2006), "Crush dynamics of square honeycomb sandwich cores", *Int. J. Numer. Methods Eng.*, **65**(13), 2221-2245.

Ye, Z.Q. and Ma, G.W. (2007), "Effects of foam claddings for structure protection against blast loads", *J. Eng. Mech.*, **133**(1), 41-47.

Yurddaskal, M. and Baba, B.O. (2016), "The effect of curvature on the impact response of foam-based sandwich composite panels", *Steel Compos. Struct., Int. J.*, **20**(5), 983-997.

Zhang, J., Wang, Z. and Zhao, L. (2016), "Dynamic response of functionally graded cellular materials based on the Voronoi model", *Compos. Part B*, **85**, 176-187.

Zheng, Z., Yu, J. and Li, J. (2005), "Dynamic crushing of 2D cellular structures: A finite element study", *Int. J. Impact Eng.*, **32**(1-4), 650-664.

Zheng, Z., Yu, J., Wang, C., Liao, S. and Liu, Y. (2013), "Dynamic crushing of cellular materials: A unified framework of plastic shock wave models", *Int. J. Impact Eng.*, **53**, 29-43.

Zheng, Z., Wang, C., Yu, J., Reid, S.R. and Harrigan, J.J. (2014), "Dynamic stress–strain states for metal foams using a 3D cellular model", *J. Mech. Phys. Solids*, **72**, 93-114.

Zheng, J., Qin, Q. and Wang, T.J. (2016), "Impact plastic crushing and design of density-graded cellular materials", *Mech. Mater.*, **94**, 66-78.

Zhou, H., Wang, X. and Zhao, Z. (2016), "High velocity impact mitigation with gradient cellular solids", *Compos. Part B*, **85**, 93-101.

Zhu, H.X., Hobdell, J.R. and Windle, A.H. (2001), "Effects of cell irregularity on the elastic properties of 2D Voronoi honeycombs", *J. Mech. Phys. Solids*, **49**(4), 857-870.

Zhu, H.X., Thorpe, S.M. and Windle, A.H. (2006), "The effect of cell irregularity on the high strain compression of 2D Voronoi honeycombs", *Int. J. Solids Struct.*, **43**(5), 1061-1078.

CC